

PAPER • OPEN ACCESS

Wake effects between two neighbouring wind farms

To cite this article: Nicolai Gayle Nygaard and Sidse Damgaard Hansen 2016 *J. Phys.: Conf. Ser.* **753** 032020

View the [article online](#) for updates and enhancements.

You may also like

- [Analyzing complex wake-terrain interactions and its implications on wind-farm performance.](#)
Mandar Tabib, Adil Rasheed and Franz Fuchs
- [Wind turbine wakes can impact down-wind vegetation greenness](#)
Jay E Diffendorfer, Melanie K Vanderhoof and Zach H Ancona
- [Wing-wake interaction: comparison of 2D and 3D flapping wings in hover flight](#)
Y J Lee and K B Lua



ECS
The
Electrochemical
Society
Advancing solid state &
electrochemical science & technology

DISCOVER
how sustainability
intersects with
electrochemistry & solid
state science research

Wake effects between two neighbouring wind farms

Nicolai Gayle Nygaard and Sidse Damgaard Hansen

DONG Energy Wind Power
Kraftværksvej 53, 7000 Fredericia, Denmark

nicny@dongenergy.dk

Abstract. We address the issue of wake effects between two neighbouring offshore wind farms by analysing simultaneous production data from Rødsand II and Nysted. The upstream wind farm is found to not just perturb the flow in its wake, but also to cause speed-ups at the positions of some downstream turbines. We use the data to perform a validation of a simple wake model for flow cases corresponding to wind directions of maximum internal and external wake effects.

1. Introduction

Offshore wind energy is currently undergoing a massive build-up of capacity. This implies a concentration of offshore wind farms in groups and clusters to harvest the optimal wind resources and exploit logistical and infrastructural synergies. The clustering of wind farms presents new challenges, as neighbouring wind farms affect one another through increased wake losses.

In previous work, the wind speed recovery behind offshore wind farms has been studied using a small number of met masts at fixed locations downstream of the turbines [1–4]. This provides a useful reference for model predictions of the wake behind a wind farm in a limited range of wind directions. However, it requires additional modelling steps to describe the performance of another, neighbouring wind farm placed in this wake. Other studies have attempted to bridge this gap by quantifying the wake loss in a wind farm, when this is downwind of a neighbouring wind farm [5,6]. Hitherto this type of analysis has been based on production data from only one of the wind farms. This makes it problematic to define the undisturbed inflow and hence the gross power, which influences the estimated wake losses. Similarly, without knowledge of the operational state of the turbines in the upstream wind farm neighbour, periods where all or some of the neighbour turbines are curtailed or stopped may inadvertently be included. This would lead to an underestimation of the wake effect of the neighbour.

Consequently, access to concurrent production data from both wind farms is required for an accurate appraisal of the mutual impact of neighbouring wind farms. Only in this way, may one define a free inflow at the most upstream position in the wind farm cluster and condition the analysis on the normal operation of turbines in both wind farms. Here, we report for the first time on the results of such an analysis. The subject of the analysis is the wind farm pair of Rødsand II and Nysted, which is located in Danish waters in the southwestern Baltic Sea. This proto-cluster consists of 162 turbines and spans 20 km from end to end. While neither wind farm consists of turbines matching those being deployed today in size or capacity, the dataset is unique and valuable, since it encompasses the periods before and after the construction of Rødsand II. This enables a direct comparison of the wake losses with and without



the neighbouring wind farm. We can assess the ability of the current generation of wake models to account for the wake effects on the regional scale of a wind farm cluster. In this paper, we narrow the scope to the predictive power of a single wake model, proposed by N. O. Jensen [7,8]. This model contains just a minimum of physics, as it conserves mass in the flow, and is selected here for its extreme simplicity. It may be speculated that more advanced wake models that include more of the relevant flow physics should perform at least as well as the N. O. Jensen model, though this is not guaranteed.

2. Wind farms

The two neighbouring wind farms Nysted and Rødsand II are situated in the Danish Baltic Sea south of the island Lolland, see Figure 1. The two wind farms are separated by a 3.3 km gap. The characteristics of the two wind farms are listed in Table 1. Since the difference in the hub height of the two parks is only 0.5 m, we neglect shear effects in this analysis.

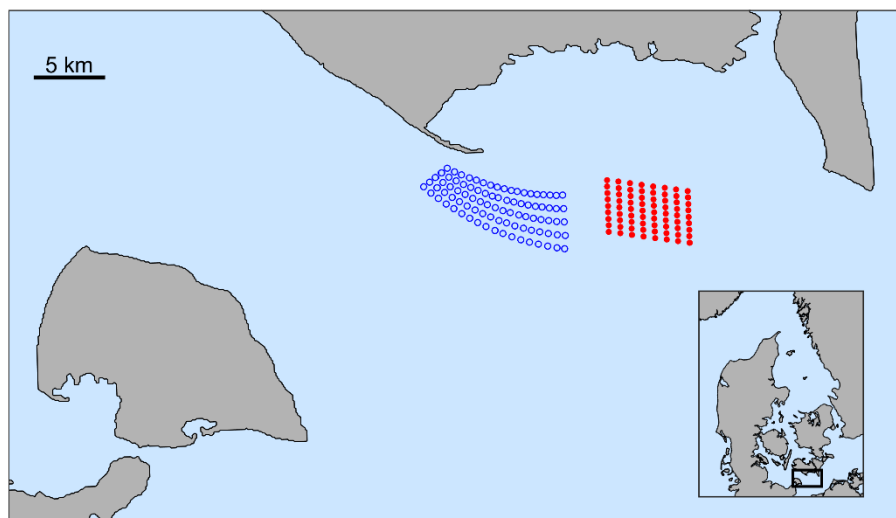


Figure 1. Map of the area with Rødsand II turbines indicated by open circles. The Nysted turbines are represented by the closed circles. The inset shows the location on a larger map.

Table 1. Characteristics of the Nysted and Rødsand II offshore wind farms.

	Nysted	Rødsand II
Turbine type	Bonus 2.3 MW Combi Stall	Siemens 2.3 MW
Rotor diameter [m]	80	92.6
Hub height [m aMSL]	68	68.5
Number of turbines	72	90
Commissioned	2003	2010

A special feature of the Nysted turbines is their two-speed generator, which gives a jump in the trust curve when the generator speed changes. This must be considered explicitly in the wake model to avoid underestimating the wake losses. The details are described in Appendix A.

Rødsand II was commissioned 7 years after Nysted. Hence we have three distinct periods with regards to wakes: a period before Rødsand II, a period where Rødsand II was under construction, and the period after Rødsand II became fully operational. These periods are listed in Table 2.

Table 2. Distinct data periods

	Time period
Rødsand II pre-construction	Before April 2010
Rødsand II construction	April 2010 - September 2010
Rødsand II post-construction	After September 2010

In this paper we focus on the periods before and after the construction of Rødsand II, where Nysted is either isolated or subjected to the full wake from Rødsand II. The period of Rødsand II construction is ignored, since in this period the wake loss from Rødsand II on Nysted is gradually increasing.

3. Data processing

For both wind farms production data were available as ten-minute averages. For Rødsand II we had access to selected production data from first power in April 2010 to April 2015. The analysis could therefore be based on multiple years of data in both the Rødsand II pre-construction phase and the in the Rødsand II post-construction period, see Table 2. The production data were filtered to remove curtailment and periods with limited turbine availability. Such events corresponds to periods of reduced turbine production that could otherwise be wrongly attributed to wakes.

No data from the met masts at Nysted or Rødsand II were available for this analysis. Instead the wind conditions had to be inferred from the wind farm production data. The wind direction was constructed from the median yaw direction of the turbines. Using the median makes the method more robust against imperfections in individual yaw sensors. Nonetheless, the median yaw direction is not a true indicator of the wind direction, since it generally contains an offset. We remove this offset by calibrating the wind direction against the expected direction of maximum power deficit between pairs of turbines. This method of wind direction calibration was introduced by Rethoré *et al* [9]. Since the offset can be time-dependent we perform the calibration in a moving time window.

The wind speed was derived for each turbine from the ten-minute average power and the manufacturer's power curve. This approach only works for wind speeds between cut-in and rated speed. Outside this range we relied instead on the nacelle anemometer. We estimated the free stream wind speed, which defines the inflow upstream of the cluster, by identifying the turbines that are unaffected by any wakes for each wind direction. The free stream wind speed was then approximated by averaging the derived wind speed at these upstream turbines that were assumed to be exposed to the undisturbed inflow. The appropriateness of this approximation depends on the homogeneity of the inflow.

4. Wind speed variations

It is illuminating to plot the variation of the wind speed across the site. This illustrates the wake effect both within the wind farms and between them in a very direct way. Additionally, due to the difference in rotor diameters between the two Rødsand II and Nysted turbines, a comparison of power values across the two wind farms is not straightforward. In this section we present patterns of the wind speed derived from the operational data. These flow patterns reflect the flow through and around the wind farms and also visualise the effect of the nearby coast. The patterns represent the average wind speed at each turbine position, when data are filtered on the wind direction and the free stream wind speed.

4.1. Wake patterns

Figure 2 shows the wind speed flow pattern when the wind direction is aligned with the east-west rows in Nysted. The two panels separate the results in the period before and after the construction of Rødsand II with the top panel representing the situation before Rødsand II was built. This is the baseline. It shows how the wind speed deficits increase in each column, when progressing further downstream. The north and south rows exhibit slightly higher wind speeds, since entrainment of the

higher speed surrounding air is accelerated for these rows, due to the reduced number of adjacent turbines. Consequently, wakes in these two rows recover faster than the wakes in the interior rows.

The bottom panel shows the wind speed pattern with both wind farms in operation. Due to the curvature of the Rødsand II rows the wind speed has a non-monotonic dependence on the turbine number along the rows. This is particularly clear for the three northernmost Rødsand II rows, where the wind speed reaches a minimum after the middle of the rows before rising again towards the back-end of the wind farm. Later, in Figure 5 and Figure 6, we will see this reflected in the turbine power.

For this wind direction sector Nysted is in the wake of Rødsand II. This has two important consequences. The first is that the wind speed deficits in the downstream wind farm are enhanced. In Figure 2 the wind speed at the Nysted turbines in the wake of Rødsand II (approximately rows 4-9 from the north) is decreased. This is clearest for the first few turbines in the affected rows. At the end of the rows, the wind speed for the post Rødsand II scenario closely resembles that before construction of the neighbouring wind farm. The additional wake losses from the other wind farm are thus confined to the first few rows in Nysted.

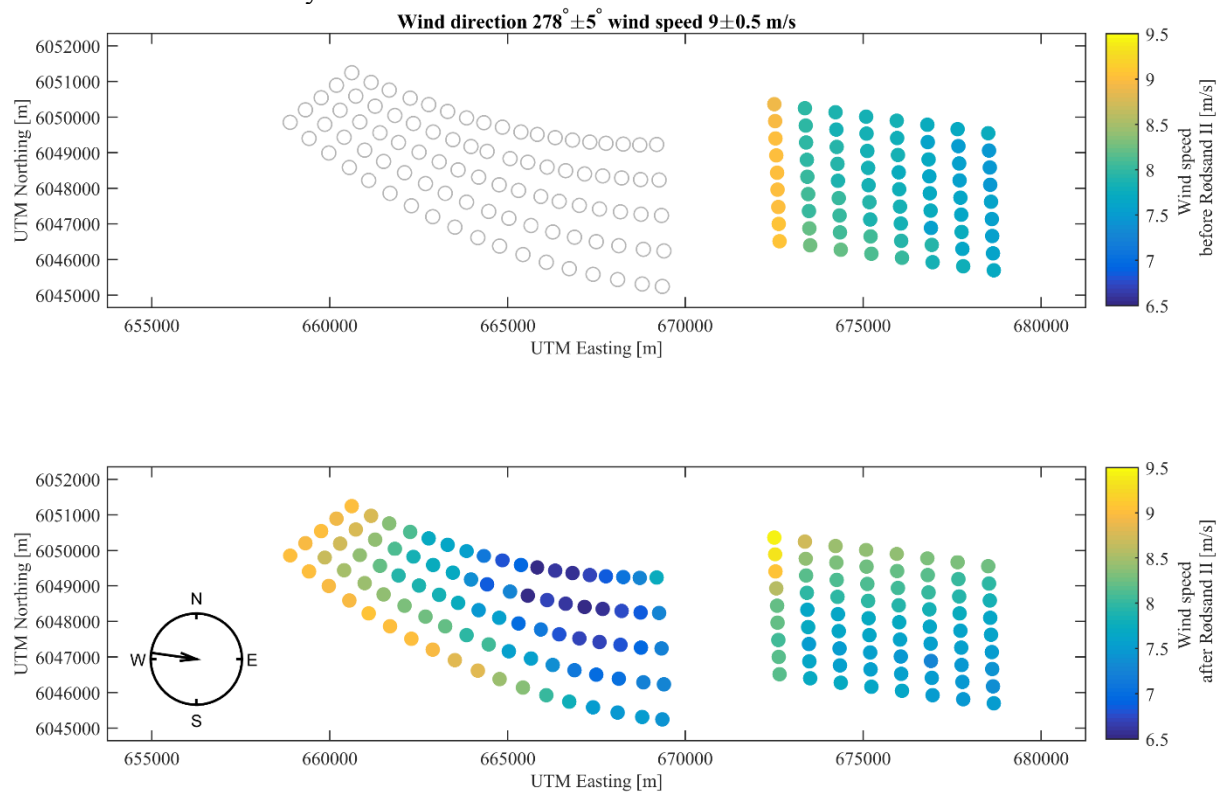


Figure 2. Wind speeds for Rødsand II (left) and Nysted (right) based on wind turbine data. Top panel: before construction of Rødsand II. Bottom panel: after construction of Rødsand II. Turbine positions are indicated by the dots, and the wind speed is represented by the colour.

4.2. Speed-up effects

An intriguing second consequence of the neighbouring wind farm is an increase of the wind speed of the Nysted turbines that are not in the wake of Rødsand II. In the example in Figure 2 this can be seen for the Nysted rows 1-3 with the strongest effect for the northernmost row. Notice in particular how the wind speed at the front turbines in the northwest corner exceeds the free stream wind speed measured at the front row of Rødsand II by almost 0.5 m/s. Since this phenomenon is absent before the construction of Rødsand II, we take this as evidence of a speed-up around the northwest corner of Rødsand II. We are not aware of any modelling result that has demonstrated this effect. Further

analysis, which is not included here, demonstrates that the speed-up is confined to a narrow wind direction range around the direction included here.

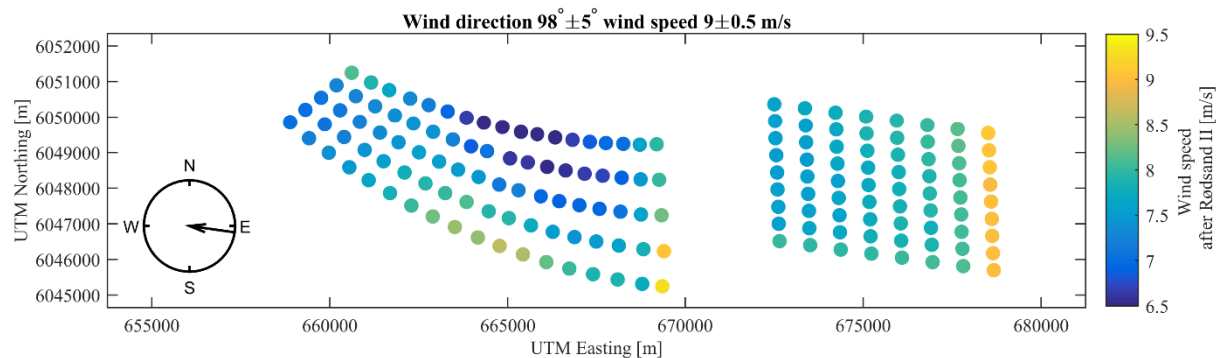


Figure 3. Same as Figure 2 for the opposite wind direction.

In Figure 3 the case where the inflow is from the east is plotted. As in the previous case, the wind direction is aligned with the Nysted rows. For such eastern winds, Rødsand II is in the wake of Nysted and the wind speed at most of the Rødsand II turbines is reduced when compared with Figure 2. However, as before there is indication of a speed-up effect, now at the southeast corner of Rødsand II. In particular, the wind speed at the turbine in the southeast corner of Rødsand II is larger than the wind speed at the front row turbines in Nysted. In this case the speed-up is 3% at 9 m/s inflow speed.

4.3. Coastal effects

When the wind is from other directions, different patterns of flow variation across the site are evident. An example is shown in Figure 4, where the wind is from the north. The variation of the wind speed among the front turbines in Rødsand II is notable. Differences of up to 16% in wind speed among free stream turbines indicate that the ambient wind speed varies significantly across Rødsand II in this wind direction. A possible explanation for this variation in the inflow velocity is coastal effects arising from differences in fetch. The coastline of the island Lolland has a triangular shape with the tip pointing towards the north-west corner of Rødsand II (see Figure 1). Accordingly, the turbines near this corner of the wind farm are the ones closest to the shore. Since the wind speed tends to increase with increasing distance from the coast [10,11], the increase in the wind speed from the northwest corner moving east along the northern face of Rødsand II is consistent with what one would expect from the shape of the coastline and the layout of the wind farm. In contrast, the northernmost row of Nysted is almost parallel with the coastline, and there is little variation in the inflow wind speeds from the north. Spatial variations in the inflow wind speed are normally not considered in wake model validations, but based on Figure 4 we observe that using an averaged free stream wind speed (or a single point measurement like a met mast) as input to a wake model can lead to large errors.

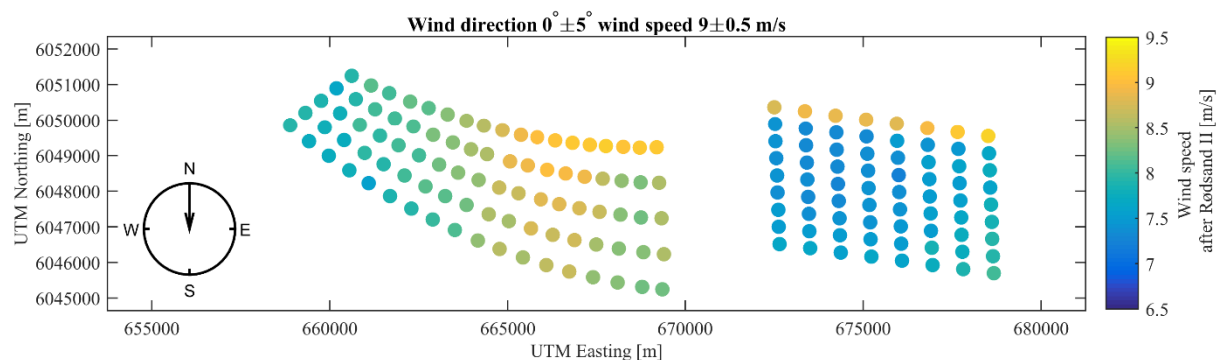


Figure 4. Same as Figure 2 for wind from the north.

5. Wake model validation

We now test how well a simple wake model predicts the power variation through the Rødsand II-Nysted mini-cluster. The N. O. Jensen wake model [7,8] includes only the most basic flow physics, yet it is still a trusted workhorse in the industry, despite the emergence of higher fidelity models. One reason for this is the simplicity of the model. As it is analytic, the N. O. Jensen model is computationally efficient, which makes it fit not only for energy yield calculations, but also for layout optimisation. This model has previously proved capable of simulating wakes in very large offshore wind farms [5]. In the two subsections below we investigate the predictive power of the model for a row of turbines spanning both wind farms. First, we test the model predictions of the spatial pattern of wakes along the row. Second, we compare the model output with the observed turbine power for a subset of the turbines as a function of the wind speed. The model is specified in Appendix B.

The thrust curve originally supplied for the Bonus 2.3 MW turbines at Nysted and used in previous wake modelling of the site assumes a sharp jump of the thrust coefficient at a fixed wind speed, corresponding to a well-defined separation between high and low rotor speeds. In reality, the rotor speed shows considerable hysteresis, and the turbines often operate at a higher thrust at low wind speeds than described by the original thrust curve, leading to a two-branch structure of the C_T curve. This contributes to the underestimation of the wake losses seen in previous studies of wakes at Nysted [4,12–17]. We detail this issue and its resolution in Appendix A. In the validation results below, we have explicitly accounted for the dual-branch thrust curve.

We analyse the wake loss along a row of turbines in both wind farms for a particular inflow wind speed and wind direction. The rows of Rødsand II are not exactly in line with those in Nysted. Nonetheless, we can choose pairs of rows across the two wind farms that are sufficiently aligned that they can be analysed together as a single transect spanning both Rødsand II and Nysted. For the results presented here we use a wind direction sector of 30° aligned with the east-west axis in Nysted. We restrict our attention to this sector size, since it is the one typically used in energy yield calculations. Furthermore, research has shown that any uncertainty on the observed wind direction will have marginal impact on the experimental power ratios for a wind direction sector of this size [18]. The wind speed bin has a width of 1 m/s. For reference, the turbines in the row are labelled from west to east R1, ..., R18 and N1, ..., N8 for those belonging to Rødsand II and Nysted, respectively.

To ensure that the true wake patterns are clearly represented we only include data, where all turbines in the chosen row operate normally. In addition, we demand that the same applies for at least 95% of all turbines in both wind farms. We could have chosen this threshold at 100%, but that severely reduces the amount of useable data, and our tests do not indicate that the results change noticeably. We therefore sacrifice a small amount of accuracy in exchange for a statistically more robust estimate. We filter the data based on the wind speed at the most upstream turbine in the row.

5.1. Spatial variation of wake losses

In Figure 5 and Figure 6 we plot for two different wind directions the power of each turbine along the analysed row when averaged over the observations consistent with the filters on the inflow parameters and the operational state. Notice that since the Nysted turbines have a smaller rotor diameter than the turbines at Rødsand II, the Nysted turbines will produce less power compared with the Rødsand II turbines at the same wind speed (when below rated speed). The wake calculation explicitly accounts for the individual power and thrust curves of the turbines.

Despite its simplicity the N. O. Jensen wake model captures the variation along the curved Rødsand II row and the recovery across the 3.3 km gap between the two wind farms reasonably well.

Notably, the model also predicts the correct wake loss towards the end of the Nysted row, provided the updated thrust curves described in Appendix A are used. This contradicts previous work stipulating the existence of a ‘deep array effect’ leading to a structural underestimation of the wake losses inside large wind farms by simple wake models like the one used here [4,12,14,15,17]. The main difference is the use of updated Nysted thrust curves in the present analysis, as can be seen by comparing the black and the grey lines in Figure 5 and Figure 6. This underscores the fact that a wake model, no matter how sophisticated in its description of the physics, cannot deliver unbiased predictions, unless it is provided with inputs, which reflect the true state of the experiment. Unawareness of the proper inputs should not be mistaken for a deficiency in the model.

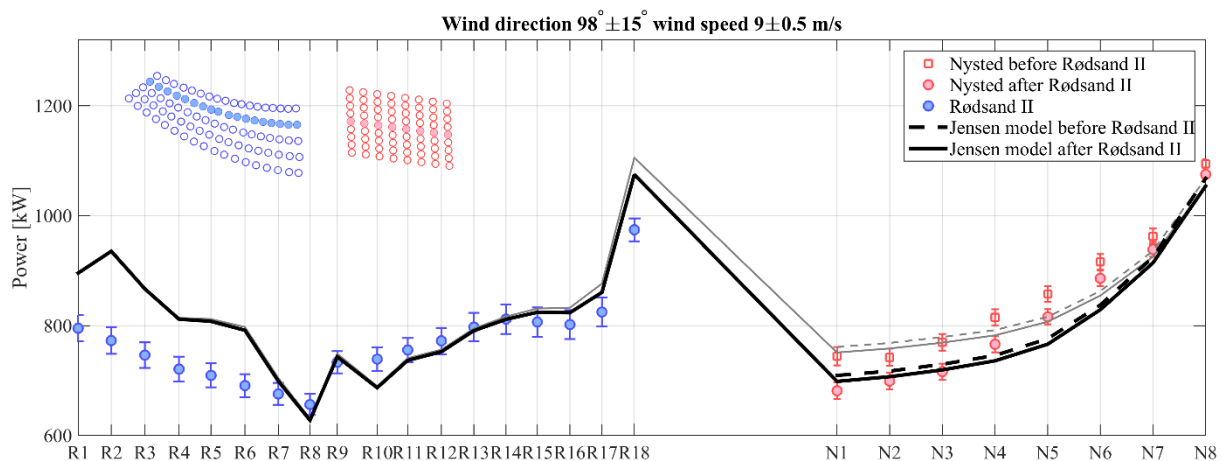


Figure 5. The power of Rødsand II and Nysted turbines along a row spanning both wind farms. Blue filled circles represent data from Rødsand II turbines, red open squares and filled circles are the observations for the Nysted turbines before and after the construction of Rødsand II, respectively. The error bars represent the 95% confidence interval on the mean value of the observations. Black lines (dashed/solid) are the results of a wake model calculation (before/after Rødsand II). Grey lines indicate the same results, when using the original Nysted thrust curve. Inset: the layout of the wind farms with the row of analysed turbines highlighted.

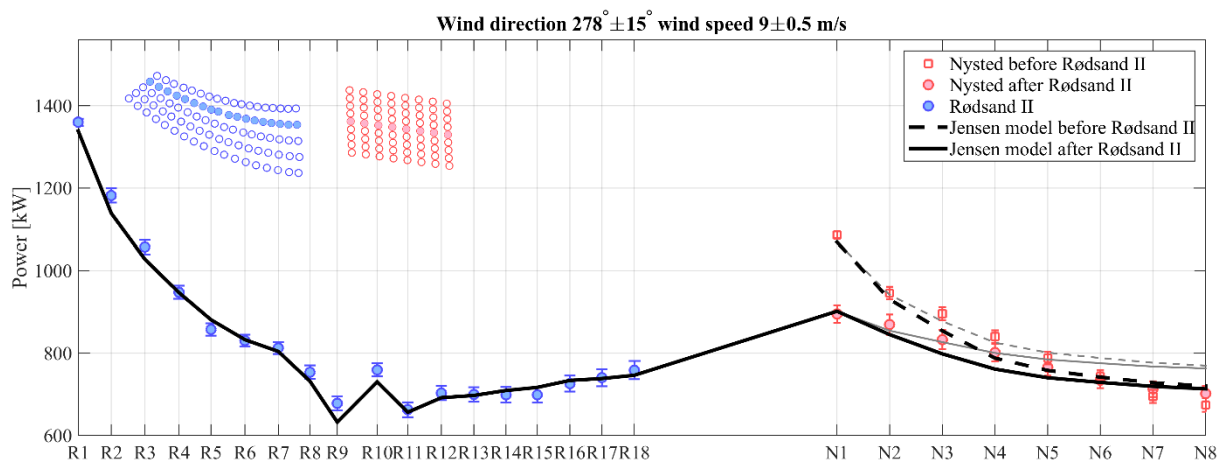


Figure 6. Same as Figure 1 but for the opposite wind direction. Before Rødsand II the inflow wind speed is taken at N1. After the construction of Rødsand II the reference turbine is R1.

Two important additional points can be made about the Nysted results. First, the pre- and post-Rødsand II results for wind directions close to 98° match each other closely, as one might have expected. This means that we can have confidence that changes in other directions between the two

periods are due to the construction of the neighbouring wind farm. Secondly, in the opposite direction the power of Nysted turbines before and after Rødsand II converge as we move deeper into Nysted along the row of analysed turbines. The implication is that the additional wake loss from Rødsand II is concentrated around the first few columns of Nysted. Sufficiently deep into the array the presence of the upstream neighbour is no longer felt. From this we anticipate that the relative influence of a neighbouring wind farm in terms of external wake losses is decreased, if we increase the physical extent of the target wind farm.

5.2. Wind speed dependence of wake losses

The model validation in the previous subsection focussed on a single wind speed. Now we test the model against observations for a range of wind speeds to investigate how the model predictive potential depends on the inflow conditions. To make the presentation clearer we have selected four turbines that represent different regions of the long row. In Figure 7 these are N1, R18, R9 and R1 and the wind is from the east. The first two of these are the last turbine in Nysted and the first turbine in Rødsand II when looking along the row in the direction of the wind. By comparing those, we can see that at most wind speeds the model provides a reasonable description of the wake recovery across the gap between the wind farms. For N1 the results before and after the construction of Rødsand II match each other closely at all wind speeds. This is encouraging, since it indicates that the two periods had similar wind conditions, which would mean that the observed wake losses are likely representative of the average conditions at the site.

For this wind direction R9 and R1 are in the middle and the back end of Rødsand II, respectively. Together with the R18 results in Figure 7 they reveal that for inflow wind speeds up to 10 m/s the model is equally accurate at the front, the middle and the back of Rødsand II. Above 10 m/s the model tends to underestimate the wake loss with the largest discrepancy at the most downstream turbines.

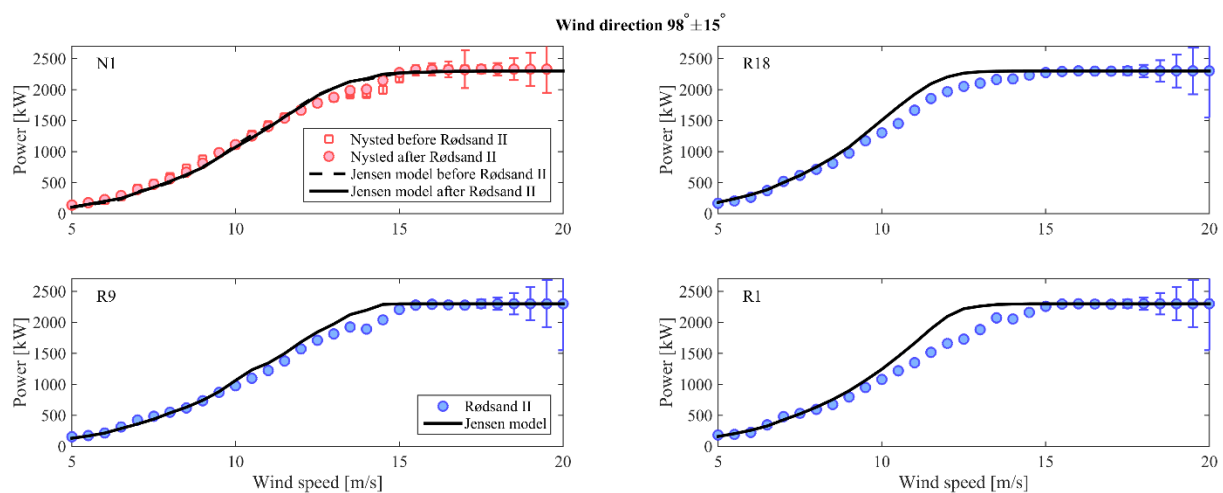


Figure 7. Power of four turbines in the row as a function of the inflow wind speed. The panels are organised in order of increasing downwind distance. Symbols represent the observations with the error bars signifying the 95% confidence interval on the mean. The model results are shown by the lines. The dashed and solid lines corresponding to the Nysted model results before and after Rødsand II are almost indistinguishable on this scale.

Figure 8 shows the case where the wind is from the west. For this case we include results for turbines R10, R18, N1 and N8. These represent turbine positions at the middle of Rødsand II, just before and after the gap between the wind farms, and at the back end of Nysted, respectively. The wake model does a remarkable job of predicting the variation of the power loss with the inflow wind speed for all Rødsand II turbines. Compared with the opposite direction the model accuracy is

improved at the end of the row (here N8). Interestingly, the discrepancy also *decreases* after the addition of Rødsand II, which makes the row 225% longer. This implies that any underestimation of the wake loss is not systematic and not proportional to the size of the wind farm.

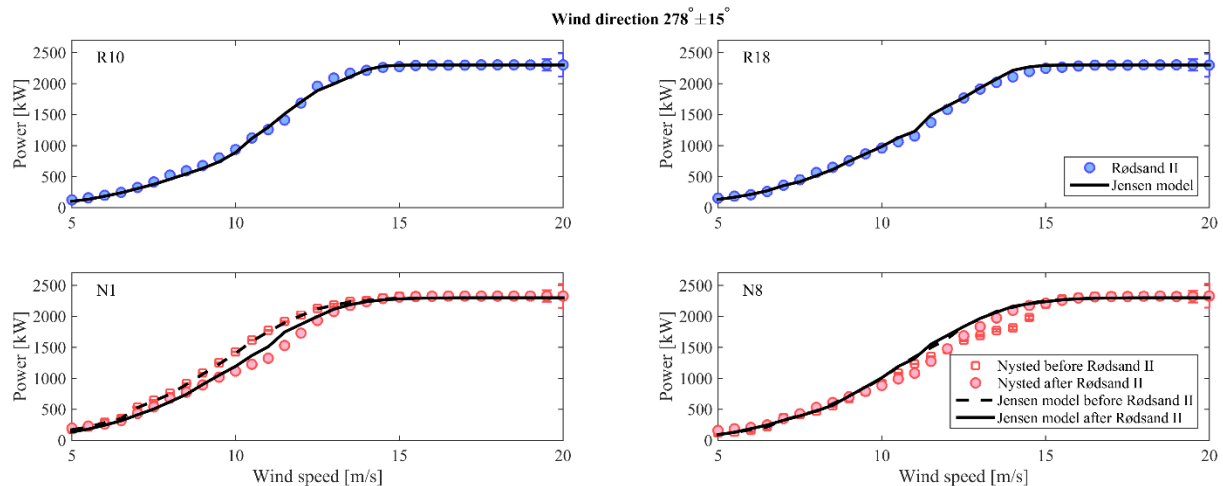


Figure 8. Same as Figure 7, but for the opposite wind direction and a different selection of turbines. Before Rødsand II the inflow wind speed is taken at N1. After Rødsand II the reference turbine is R1.

In Figure 2 we observed the reduction of the wind speed due to the upstream wind farm. The effect on the power production is clear for N1 in Figure 8 from the separation between the pre-Rødsand II and post-Rødsand II results. But comparing the panels for N1 and N8 we see as in the previous subsection that the curves for Nysted before and after the construction of Rødsand II converge towards the back end of the wind farm. The upstream neighbour therefore mainly exerts its influence on the front turbines of the downstream wind farm.

6. Conclusions

We have analysed the case of two neighbouring offshore wind farms and compared observations with a simple wake model. This type of analysis is crucial to understand the interaction between constituents of wind farm clusters currently under construction or in planning. Nysted and Rødsand II represent a unique system in this regard, since the dataset covers both the pre- and post-Rødsand II periods. This enables a direct comparison of the wake losses with and without the neighbour.

In general, the predictions of the simple wake model we have tested are in good agreement with the observations. However, the usefulness of the model for large offshore wind farms has been put into question by prior assertions that the model systematically underestimates the wake losses inside large wind farms. The existence of such a ‘deep array effect’ would imply that the model was insufficient or needed corrections. In this study, we find no evidence of a systematic deep array effect, despite comparing the model with observations along a row of 26 turbines! This matches the conclusion of previous research on other large offshore arrays [5]. When comparing the Nysted wake losses before and after Rødsand II, we find that the additional wake loss from the neighbouring wind farm is roughly confined to the first few rows in the downstream wind farm.

The analysis has revealed that the modelling as well as the interpretation of the experimental results is subject to complications. For Nysted we found that the turbines may operate at two discrete rotor speeds for a given wind speed, which implies that wakes are generated subject to two distinct thrust curves. The original thrust curve assumes that the turbines switch from low to high rotor speed at a fixed wind speed with no overlap of the two operational modes. To remedy this discrepancy we have utilised updated thrust curves and a time series approach to wake modelling.

Another issue is the variations in the inflow conditions across the site. We speculate that the large variations observed for northern winds are related to coastal gradients driven by differences in fetch. Such variations make it difficult to define the free stream wind speed reliably from the conditions at the front row turbines. In addition, since the wind speed may continue to develop through the wind farm, it is also an open question, how such spatial variation in the wind resource is accounted for in the wake model. On a similar note, we also observed a speed-up of the wind relative to the inflow speed at some turbine positions in the downstream wind farm. Regardless of how these questions are resolved, the major issue here is how to account for a wind speed gradient in a wind resource assessment. Future reductions of the uncertainty in energy yield calculations might well be driven by understanding this issue and less by improvements in wake modelling.

References

- [1] L. E. Jensen, C. Mørch, P. B. Sørensen, and K. H. Svendsen, in *Proc. Eur. Wind Energy Conf. London* (2004).
- [2] S. Frandsen, R. Barthelmie, O. Rathmann, H. E. Jørgensen, J. Badger, K. Hansen, P. Rethore, S. E. Larsen, and L. E. Jensen, *Risø-R-1615(EN) Summary Report : The Shadow Effect of Large Wind Farms : Measurements , Data Analysis and Modelling* (2007).
- [3] J. L. Philips, S. D. Cox, A. R. Henderson, and J. P. Gill, in *Proc. Eur. Wind Energy Conf. Warsaw* (2010).
- [4] G. M. Smith, A. Neubert, and W. Schlez, in *Proc. EWEA Offshore, Amsterdam* (2011).
- [5] N. G. Nygaard, *J. Phys. Conf. Ser.* **524**, 012162 (2014).
- [6] K. S. Hansen, P.-E. Réthoré, J. Palma, B. G. Hevia, J. Prospathopoulos, A. Peña, S. Ott, G. Schepers, A. Palomares, M. P. van der Laan, and P. Volker, *J. Phys. Conf. Ser.* **625**, 012008 (2015).
- [7] N. O. Jensen, *A Note on Wind Generator Interaction, Risø-M-2411* (1983).
- [8] I. Katic, J. Højstrup, and N. O. Jensen, in *Proc. Eur. Wind Energy Conf. Rome* (1986).
- [9] P.-E. Réthoré, N. A. Johansen, S. T. Frandsen, R. Barthelmie, K. S. Hansen, L. E. Jensen, and J. R. Bækgaard, M. A.B. Kristoffersen, in *Proc. Eur. Offshore Wind Conf. Stock.* (2009).
- [10] R. J. Barthelmie, J. Badger, S. C. Pryor, C. B. Hasager, M. B. Christiansen, and B. H. Jørgensen, *Wind Eng.* **31**, 369 (2009).
- [11] M. Dörenkämper, M. Optis, A. Monahan, and G. Steinfeld, *Boundary-Layer Meteorol.* **155**, 459 (2015).
- [12] W. Schlez and A. Neubert, in *Proc. Eur. Wind Energy Conf. Marseille* (2009).
- [13] R. J. Barthelmie, S. C. Pryor, S. T. Frandsen, K. S. Hansen, J. G. Schepers, K. Rados, W. Schlez, A. Neubert, L. E. Jensen, and S. Neckelmann, *J. Atmos. Ocean. Technol.* **27**, 1302 (2010).
- [14] AWS Truepower, *The openWIND Deep-Array Wake Model Development and Validation* (2011).
- [15] GL Garrad Hassan, *WindFarmer V5.0 Validation Report* (2012).
- [16] J. Cleve, M. Greiner, P. Enevoldsen, B. Birkemose, and L. Jensen, *Wind Energy* **12**, 125 (2009).
- [17] R. J. Barthelmie and L. E. Jensen, *Wind Energy* **13**, 573 (2010).
- [18] M. Gaumont, P.-E. Réthoré, S. Ott, A. Peña, A. Bechmann, and K. S. Hansen, *Wind Energy* **17**, 1169 (2013).

Acknowledgements

We thank E.ON and SEAS-NVE for kindly providing data from Rødsand II and Siemens Wind Power for the recalculated thrust coefficients for Nysted.

Appendix A - Nysted trust curve

The Bonus 2.3 MW turbines at Nysted have active stall power control. The Nysted turbines have two-speed generators and therefore operate at two distinct rotor speeds: 11 RPM at low wind speeds and 16.5 RPM at intermediate to high wind speeds. When operating at a fixed rotor speed the turbine imposes an almost constant thrust on the flow. With increasing wind speed, the C_T value will therefore tend to decrease inversely proportional to the square of the wind speed. Each fixed rotor speed of the Bonus turbines leads to a decreasing thrust curve with increasing wind speed. Thus when the generator shifts to the higher speed, the Nysted thrust curve jumps to a higher C_T value. For the original thrust curve this happens at between 7 and 8 m/s, as illustrated in Figure 9 by the black crosses. For comparison, the thrust curve of the Rødsand II turbines is also included.

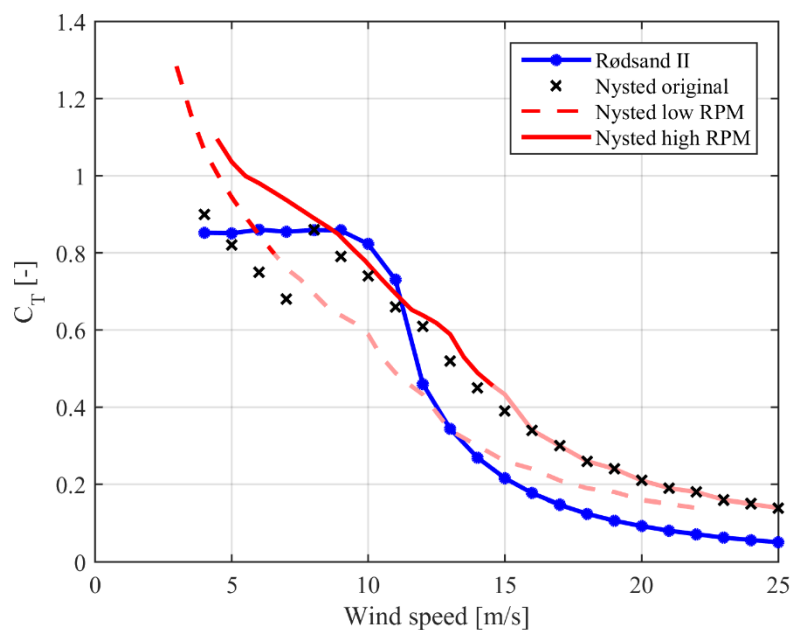


Figure 9. Thrust curves for Rødsand II and Nysted. The extrapolated values of the Nysted thrust curves specific for high and low rotor speeds are marked with the faint solid and dashed lines, respectively.

The original Nysted thrust curve gives the impression that the rotor speed jumps sharply from the low speed operation to the high-speed regime as the wind speed is increased beyond 7 m/s. However, this is not the case. In reality, there is a significant range of wind speeds, where the turbine may operate at either of the two rotor speeds as evidence by Figure 10. This hysteresis must be accounted for in wake simulations.

If the rotor speed remains high at wind speeds below the discontinuity in the thrust curve, the actual thrust coefficient should be higher than that indicated by the original curve. This corresponds to the turbines extracting a larger fraction of the available momentum from the wind. Consequently, a wake model calculation using the original thrust curve at wind speeds below 8 m/s will underestimate the internal wake losses in Nysted, since for a large fraction of the time the turbines will be operating at the higher rotor speed.

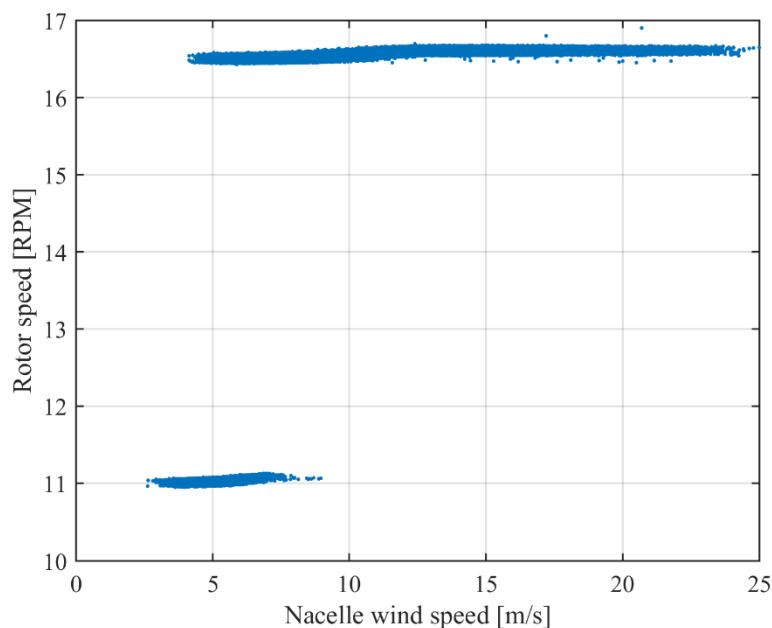


Figure 10. Rotor speed of the Nysted turbines as a function of wind speed. The relative weighting between the two branches in the wind speed range of overlap is about half and half.

To remedy this discrepancy between the original thrust curve and the observed rotor speed curves of the Nysted turbines, Siemens Wind Power has recalculated the thrust curve for the Nysted turbines using modern aero-elastic tools (*private communication*). Separate branches have been derived for the high- and low rotor speed operational states. These are included in Figure 9 as the solid and dashed lines, respectively. We have extrapolated the recalculated thrust curves to cover all wind speeds up to 25 m/s. The extrapolated parts of the curves are shown with a fainter colour in Figure 9.

These dual, overlapping thrust curves make the simulations of the Nysted wakes more complicated. At a given instant some turbines in the array may be operating at the high rotor speed and correspondingly at the upper thrust curve, while other turbines, even at the same wind speed, are in the lower rotational speed mode and exert a smaller thrust force. This can only be accounted for in the wake calculation by assigning individual thrust curves to the turbines depending on their rotor speed for every ten-minute data point. We therefore run the simulations in a time-series manner, where we perform separate wake calculations for each ten-minute data point with the corresponding inflow wind speed, wind direction *and* turbine rotor speeds as inputs. Subsequently, all simulation results are averaged in the same way as the observations.

The recalculated Nysted thrust curves exceeds unity at low wind speeds. When this happens the flow enters a turbulent wake state, where the simple momentum theory of rotor performance is invalid. In this regime we replace in the N. O. Jensen wake model the induction term $\sqrt{1 - C_T}$, which describes the ratio between the wind speed immediately behind the rotor and the free stream wind speed, by $\sqrt{C_T - 1}$. This follows the simple empirical relation between thrust and induction proposed by Leishman in *Advances in Wind Energy Conversion Technology*, Springer 2011.

Appendix B – N. O. Jensen wake model

Wake models come in many different flavours and levels of complexity. For any particular model multiple variations are usually possible with subtle differences in the implementation. It is therefore important to specify the model carefully, when reporting on comparisons between experimental results and a particular model, as the conclusions may not transfer to other wake models or different implementations of the same model.

In this appendix we describe the implementation of the N. O. Jensen wake model, which we have used in the validation analysis. The model has been implemented by DONG Energy following the original formulation by Jensen [7] and by Kátic *et al* [8]. We have confirmed that our implementation of the model is identical to the PARK model in WASP (*DTU Wind Energy, private communication*).

The basic assumption of the N. O. Jensen model is a linear expansion of the wake. Combined with conservation of mass and the linear momentum theory, which determines the initial deficit behind the rotor, this gives a wind speed deficit at a downstream turbine of

$$\delta_{ij}(X) = \left(1 - \frac{U_i}{U_0} \sqrt{1 - C_T(U_i)}\right) \left(\frac{D_i}{D_w}\right)^2$$

The wake diameter is $D_w = D_i + 2kX$, where X is the separation between the upstream and downstream rotors and k is the wake decay constant. We have used $k = 0.04$ throughout this paper. The rotor diameter of the upstream turbine is D_i , while the thrust coefficient C_T is evaluated at the inflow wind speed U_i at the upstream turbine. For an unwaked turbine U_i equals the free stream wind speed U_0 . In the present context the turbines in the two wind farms have nearly identical hub heights. Consequently, shear effects can be ignored and are not included here.

Outside the wake cone the wind speed equals that of the ambient flow. Inside the wake the wind speed is constant. To account for the partial overlap between the wake and the downstream rotor a weighted deficit is defined as $\delta'_{ij}(X) \equiv \delta_{ij}(X)A_{\text{overlap}}/A_R$. Here A_{overlap}/A_R is the fraction of the downstream rotor area covered by the wake.

If multiple wakes overlap at the position of turbine j the combination of their deficits is calculated as the quadratic superposition

$$\delta_j = \sqrt{\sum_{i \text{ upstream}} \delta'^2_{ij}}$$

The effective rotor-averaged wind speed at turbine j follows as $U_j = U_0(1 - \delta_j)$. This is used as the input wind speed for calculating the wake behind turbine j and for calculating its power production.

Finally, the model includes the assumption that when the wake impacts the surface, it is reflected. The reflected wake is treated independently. It is modelled by including for each turbine an image turbine mirrored in the surface. Hence the image turbines have negative hub height. The image turbine wakes are included in the calculation of overlapping wakes on equal terms with the direct wakes.